

Metallurgical Analysis of Failed AISI 304L Stainless Steel Tubes Used in Launch Vehicle Applications

Sushant K. Manwatkar¹ · Kailas S. Kuhite² · S. V. S. Narayana Murty¹ · P. Ramesh Narayanan¹

Received: 17 July 2015 / Revised: 3 October 2015 / Accepted: 14 October 2015 / Published online: 3 November 2015
© Springer Science+Business Media New York and ASM International 2015

Abstract Two numbers of AISI 304L stainless steel tubes with Ø6 and Ø4 mm used in pressurisation system module of a liquid engine of a satellite launch vehicle were found to crack after the qualification level random vibration test. The module has undergone resonance survey, sinusoidal vibration, and random vibration along two different axes before the occurrence of failure. The tubes failed during third-axis random vibration test. The failed tubes were subjected to detailed metallurgical analysis to understand the reasons for failure. The location of failure in both tubes was at the cross-section change area in the nipple. Cross-section change was provided in the design to reduce the diameter of the nipple to suit to tube diameter for welding. The cross-section change in the nipple acted as stress concentration resulting in the initiation of fatigue cracks. The presence of sharp-cornered inclusions in the material helped easy crack initiation. Smaller radius and angle at the weld–parent interface resulted in additional stress concentration. The presence of striations on the fracture surface and slip bands near to the fracture edge confirm that the failure of tubes to be due to vibration induced fatigue.

Keywords AISI 304 stainless steel · Vibration testing · Fatigue failure · Fatigue striations · Stress concentration · Inclusions

Introduction

Owing to their excellent combination of corrosion resistance, formability, and weldability, austenitic stainless steels [1–3] are widely used for fabrication of liquid propellant fuel feed lines and pressurization lines in liquid engines of satellite launch vehicles. In one such critical application, two sections of AISI 304L stainless steel tubes of Ø6 and Ø4 mm (internal diameter) with 1-mm wall thickness have been used. The specification of the tubes corresponds to ASTM A269-04. The chemical composition of the tubes is given in Table 1. The tubes were in bright-annealed condition. The mechanical properties of the tube are UTS: 595 MPa, 0.2YS: 306 MPa, percentage elongation (GL of 50 mm) 52, and hardness: 72 HRB. The tubes were hydro pressure tested up to 1000 PSIG. Stainless steel tubes were welded to stainless steel nipples to act as interfaces for obtaining leak-tight joints of dissimilar cross sections. During the qualification level random vibration test, the tubes were found to be broken at nipple at the location of cross-section change. The tube lines along with the module have undergone resonance survey, sinusoidal vibration, and random vibration along two different axes before failure. The tubes have failed during third-axis random vibration test. In order to understand the reasons for failure and to suggest remedial measures to avoid its recurrence, the failed tubes were subjected to detailed metallurgical analysis. This paper summarizes the analysis performed to understand the reasons for failure.

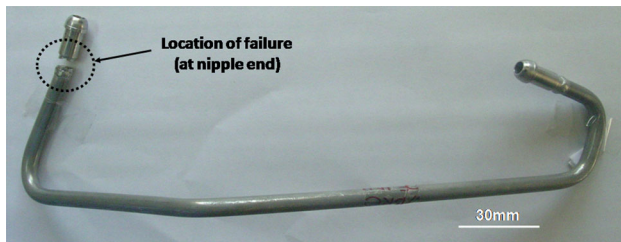
✉ S. V. S. Narayana Murty
susarla.murty@gmail.com

¹ Materials and Metallurgy Group, Material Characterization Division, Vikram Sarabhai Space Centre, Trivandrum 695 022, India

² CSC, Liquid Propulsion Systems Center, Valiamala, Trivandrum 695 547, India

Table 1 Chemical composition of the AISI 304L tubes

C	Mn	Si	Ni	Cr	Mo	P	S	Fe
0.014	1.30	0.40	10.32	18.55	0.27	0.025	0.004	Bal

**Fig. 1** Photograph showing the full view of the failed Ø6 tube

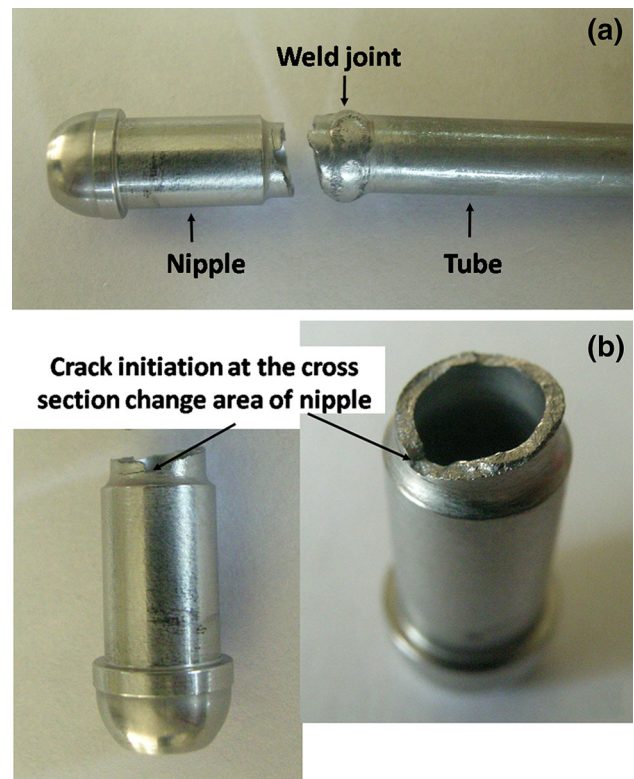
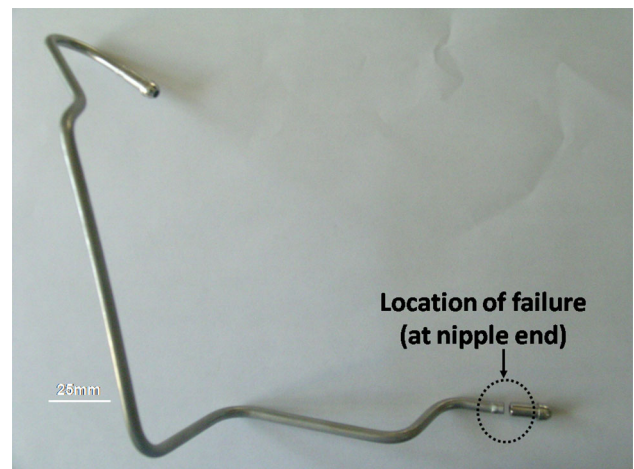
Experimental

The fracture surfaces of the failed tubes were observed in a scanning electron microscope (SEM) equipped with an energy dispersive spectrometer (EDS). For optical microscopy, specimens were sectioned vertically along the length, mounted in bakelite, and were conventionally polished using a series of emery papers and finish polished with a one micron diamond paste. The freshly polished specimens were etched electrolytically using 10% oxalic acid in water to reveal the microstructure. The specimens were observed for microstructural features and photographs were recorded using a digital camera attached to the microscope.

Results

Visual observations

The AISI 304L stainless steel tubes of Ø6 and Ø4 mm which failed during the vibration test were visually observed for details with respect to location of cracking. The failure was near to the weld joint (Figs. 1, 2, 3 and 4). Observations on Ø6 mm tube indicated that the primary crack initiated at the cross-section change area of the nipple and propagated partially in the plane of cross-section change area but deviated toward the weld side of the nipple (Fig. 2). On the other hand, in the case of Ø4 mm tube, the crack initiated at the cross-section change area of nipple and propagated in the same plane. In this case, no deviation of crack path was observed (Fig. 4).

**Fig. 2** Photograph showing the location of the failure in Ø6 tube**Fig. 3** Photograph showing the full view of the failed Ø4 tube

SEM Observations

The SEM observations on the overall fracture surface of Ø6 mm nipple indicated primary crack initiation at the cross-section change area and its propagation partially in

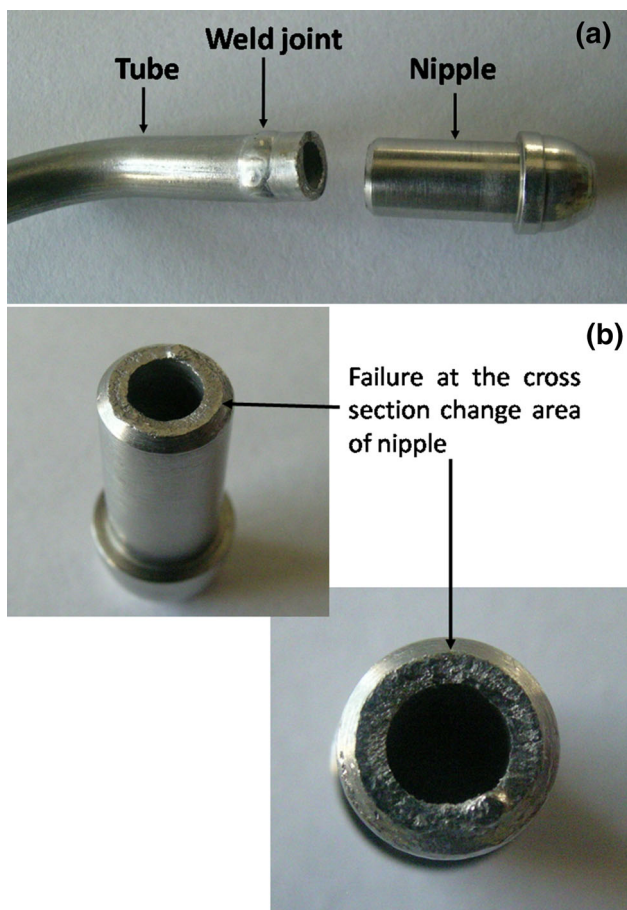


Fig. 4 Photograph showing the location of the failure in Ø4 tube

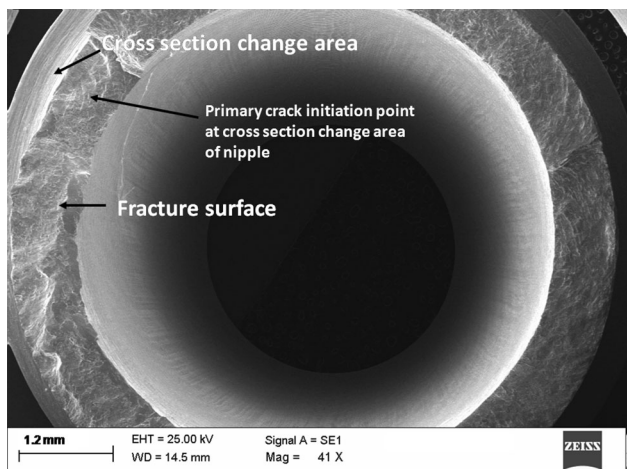


Fig. 5 SEM photograph showing the overall view of fracture surface of Ø6 nipple. The primary crack initiation can be seen on inner surface of nipple

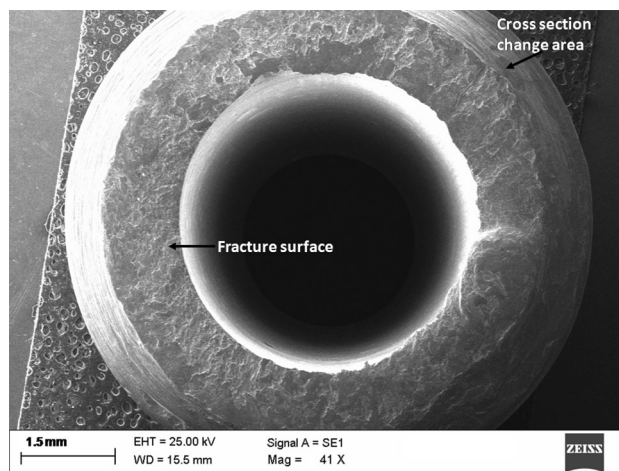


Fig. 6 SEM photograph showing the overall view of fracture surface of Ø4 nipple. Fracture initiation and propagation at the cross-section change area

the same plane and subsequent deviation of fracture path toward weld side of the nipple (Fig. 5). However, the observation on the Ø4 mm nipple indicated that the fracture initiation and propagation on the plane of the cross-section change area only (Fig. 6).

The observation on fracture surface of Ø6 mm nipple revealed the fatigue crack initiation from outer diameter side of the nipple and fatigue striations were observed at crack initiation (Fig. 7). The inclusions were also present at the location of crack initiation (Fig. 8). Fractographic observations at different areas clearly revealed the presence of fatigue striations throughout the fracture surface (Fig. 9). Micro cracks were also observed at several regions of striations (Fig. 10). Some of the striated areas indicated that the secondary cracks initiated at the sharp-cornered inclusions on the fracture surface of Ø6 mm nipple (Fig. 11). The presence of dimples on small area is attributed to the last ligament of the material which failed due to overload (Fig. 12).

The fatigue crack origin on fracture surface of Ø4 mm nipple could not be located as a significant area of fracture surface was damaged due to mechanical rubbing after failure. However, fatigue striations could be observed throughout the undamaged areas on the fracture surface (Fig. 13). Micro cracks were also observed at several regions of fatigue striations (Fig. 14).

Most of the fracture surface (about 40% fracture surface for Ø6 mm and about 60% of fracture surface for Ø4 mm) was mechanically rubbed and fractographic features were

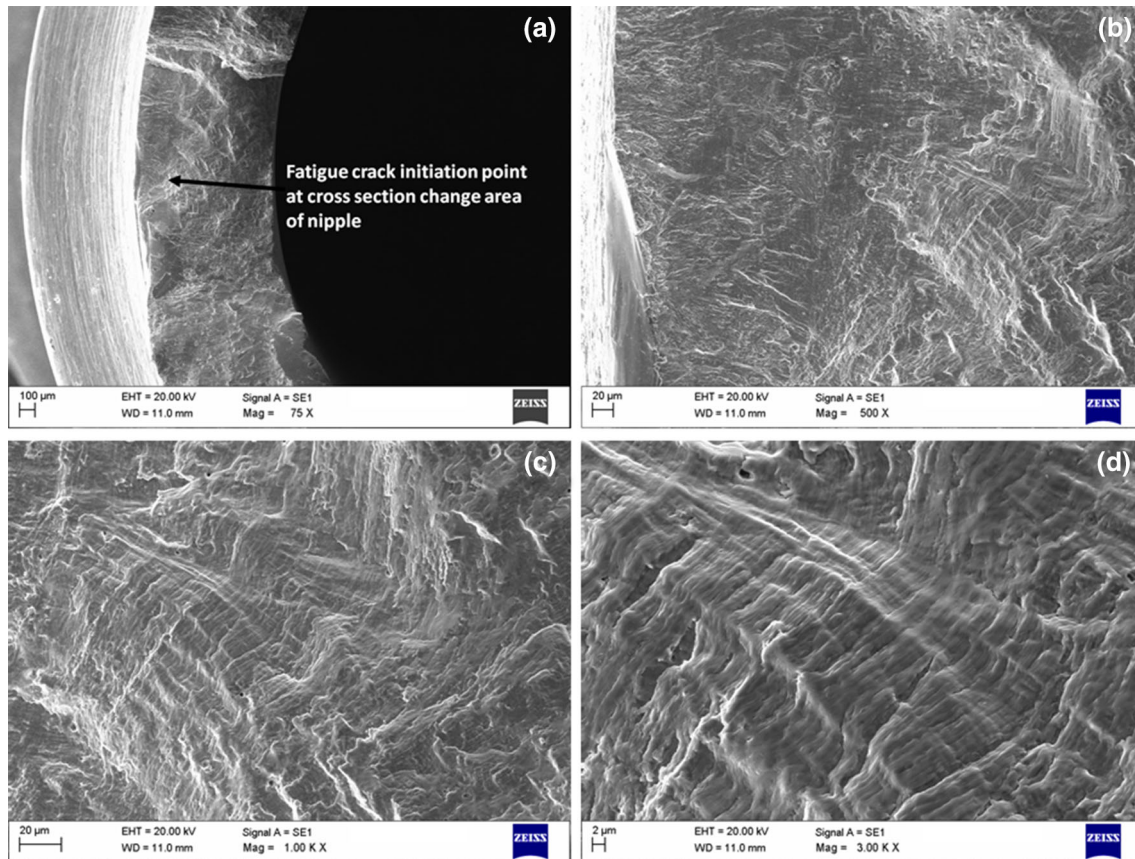


Fig. 7 SEM photograph showing the features on fracture surface of Ø6 nipple at fatigue crack initiation location at different magnifications

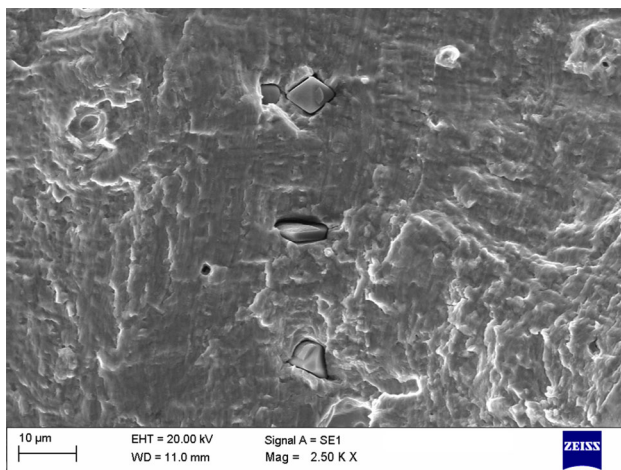


Fig. 8 The presence of non-metallic inclusions at crack initiation location of Ø6 nipple

lost; the remaining areas of the fracture surface revealed the presence of fatigue striations. This indicates that the failure occurred during the vibration test and the fracture surface was rubbed after the failure.

Optical Microscopic Observations

Optical microscopic observations on the unetched specimen of Ø6 and Ø4 mm nipple indicated a large number of sharp-cornered inclusions as shown in Fig. 15. The EDS analysis on the sharp-cornered inclusions and globular inclusions indicated similar chemical composition. The size of inclusions was in the range of 8–10 µm. The chemical composition of inclusions corresponds to the mixed oxide type inclusion (Fig. 16). Observations at the weld joint indicated the presence of a micro crack at weld–parent interface in Ø6 mm joint, whereas no cracks were observed at weld–parent interface in Ø4 mm joint (Fig. 17). Large variation in weld bead thickness was observed between Ø6 and Ø4 mm tube joint as shown in Fig. 17. The weld bead thickness in Ø6 mm plumbing joint was 3 times the tube wall thickness, whereas Ø4 mm plumbing joint has weld bead thickness 1.5 times the tube wall thickness. The angle between the weld bead and parent was measured to be 105° in case of Ø6 mm joint and 150° in Ø4 mm joint (Fig. 18). The radius at the weld–parent interface was found to be 66 µm in Ø6 mm tube

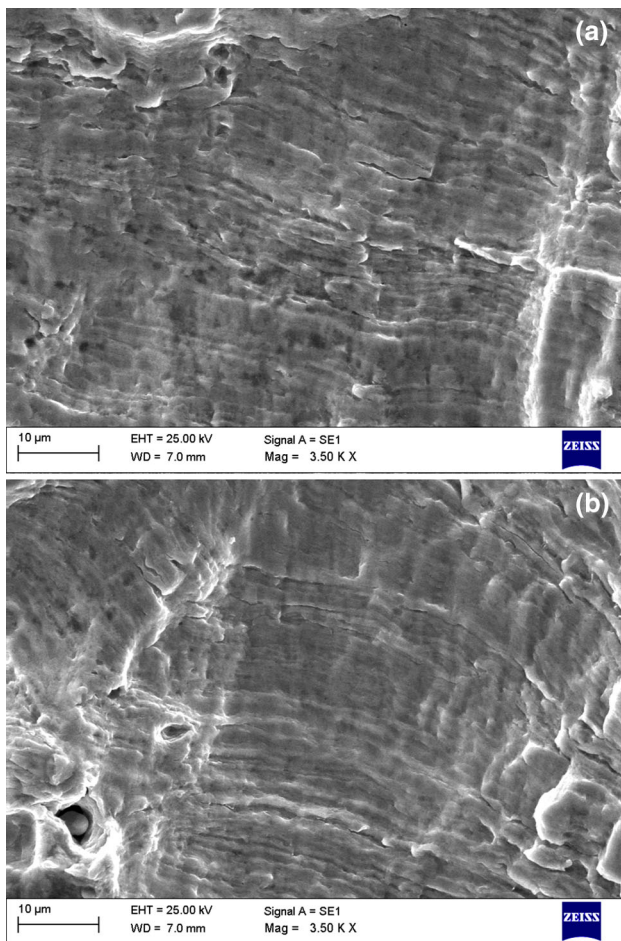


Fig. 9 SEM photograph showing the fatigue striations on fracture surface of Ø6 nipple

joint, whereas the radius in Ø4 mm tube joint was 455 µm (Fig. 19). The microstructural observations at the fracture edge revealed the presence of slip bands formed due to fatigue (Fig. 20). Microstructure consisted of austenite grain structure typical of AISI 304L stainless steel.

Discussion

The failure of the tubes occurred during the qualification level random vibration test and the location of failure was at the cross-section change area in the nipple. This observation indicated that the crack was initiated at the cross-section change radius of the nipple in both Ø6 and Ø4 mm tube joint. The location of crack initiation at the cross-section change area is due to the stress concentration. In

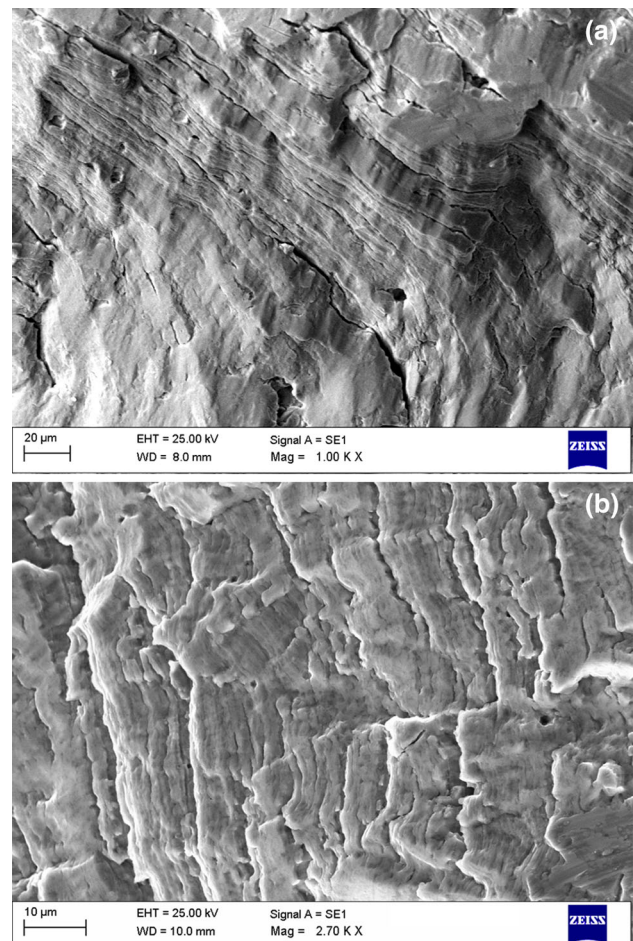


Fig. 10 SEM photograph showing the microcracks at the fatigue striations on fracture surface of Ø6 nipple

Ø6 mm tube, the primary crack was initiated at the cross-section change area and deviated in its path during propagation. However, in case of Ø4 mm tube, the crack initiated at cross-section change area and propagated in the same plane. The crack path deviation observed in Ø6 mm joint could be related to the presence of sharp-cornered non-metallic inclusions in the material.

Inclusions are undesirable but unavoidable in conventional stainless steels. Non-metallic inclusions in stainless steels can be divided into two groups viz. indigenous due to the reactions taking place in the molten steel and exogenous due to slag, refractories, or other materials with which the molten steel comes into contact [4]. Exogenous inclusions are usually larger than the indigenous inclusions and therefore, are more detrimental since they have a direct bearing on the mechanical properties especially under

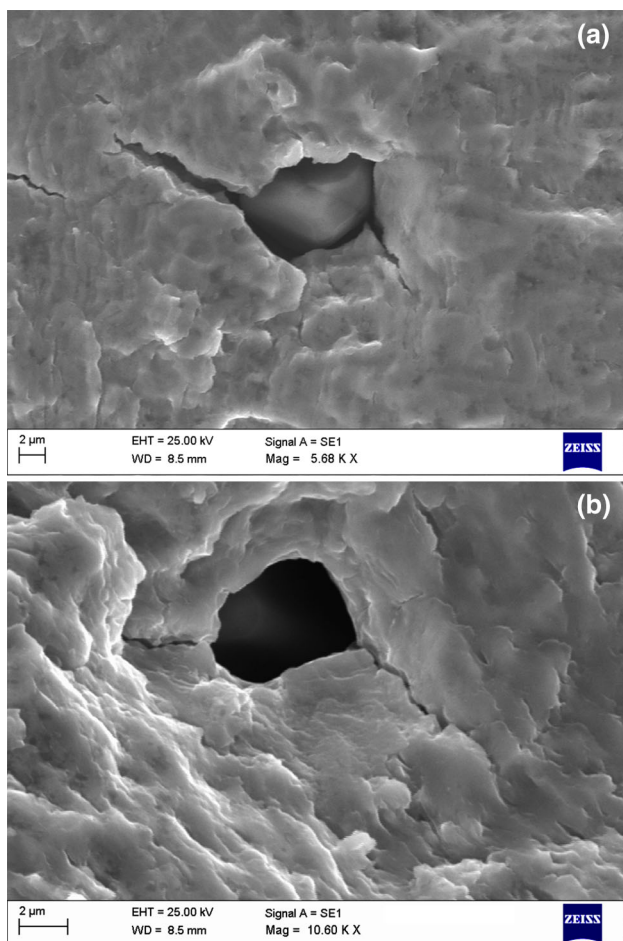


Fig. 11 SEM photograph showing the secondary cracks initiating at the sharp-cornered inclusions present on the fracture surface of $\varnothing 6$ nipple

dynamic loading conditions [5]. In the present case, no exogenous inclusions were found. The inclusions were indigenous in nature as confirmed by the EDS analysis, indicating the composition of inclusions consisted of mixed oxide of Cr, Mn, Fe, and Al (Fig. 16 a and b).

The effect of inclusions on the fatigue properties depends on their size, shape, thermal and elastic properties, and its coherency with the matrix. These factors are related to the stress concentration and stress distribution around the inclusion. Inclusion size has a major effect on the fatigue strength. Several attempts have been made [6–9] to determine the critical inclusion size under which they do not influence the fatigue strength. Duckworth and Ineson [6] have artificially introduced Al_2O_3 inclusions in steel and the critical inclusion size for an inclusion located just

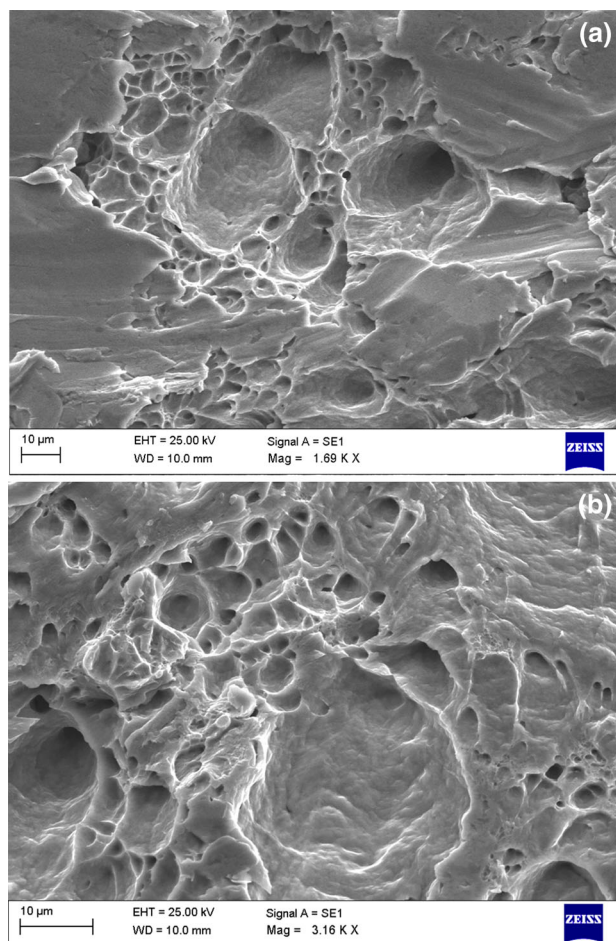


Fig. 12 SEM photograph showing the dimples on the small area of fracture surface of $\varnothing 6$ nipple, which failed at last due to overload

below the surface was found to be 10 μm . Nishijima et al. [7] studied fatigue behavior in tempered martensitic steels and concluded that the critical size of inclusions was 45 μm in the rotating bending fatigue tests. Melander and Ölund [8] reported that Ti(C,N) inclusions and alumina inclusions as small as 3 and 17 μm in size, respectively, were found on the fracture surfaces of fatigue test specimens of bearing steels. Based on their studies, it was concluded that Ti(C,N) inclusions were as detrimental to fatigue life as oxide inclusions of approximately three times their size.

Inclusions with an irregular shape and sharp edges cause larger stress concentrations around the inclusions than inclusions with a round shape which make it easier for a fatigue crack to initiate. This makes it easy for a fatigue

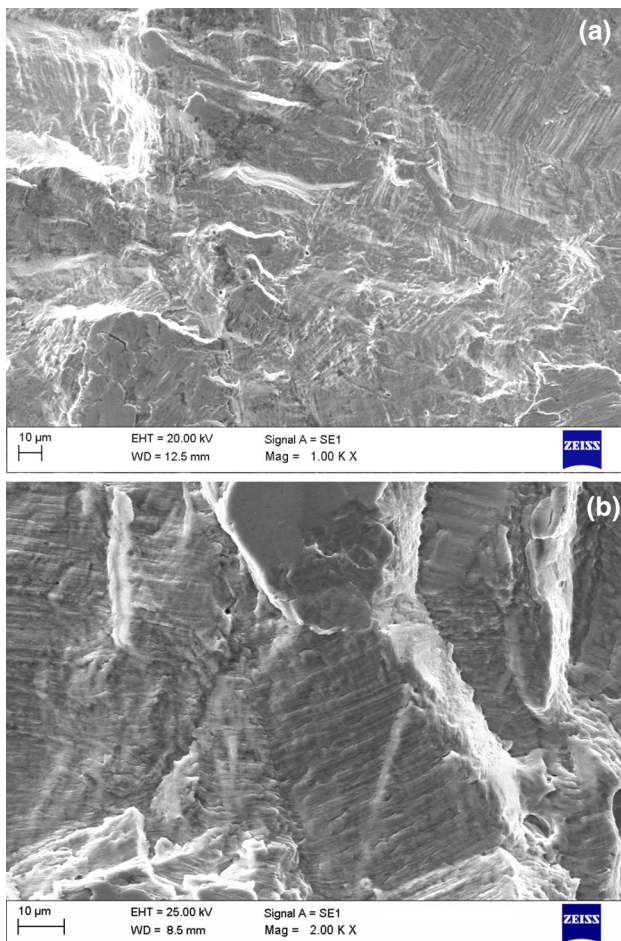


Fig. 13 SEM photograph showing the fatigue striations on fracture surface of Ø4 nipple

crack to initiate from the inclusion–matrix interface. The fatigue crack initiation is usually faster in the materials where a crack initiates from a cracked inclusion than in materials where a crack initiates from the inclusion–matrix interface [9]. However, in the present case study, cracked inclusions were not observed. Fatigue crack may initiate from the interface between the inclusion and the matrix or the inclusion itself may crack. Fatigue crack initiation is dependent on the stress concentration factor of the defect. During cyclic loading, local plastic flow can take place under the influence of stress concentration which can lead to fatigue crack initiation. When defects having the same size but different shape are compared, fatigue cracks initiate earlier from a sharp crack, than, for example, a round hole, which usually means that the fatigue life is shorter, when the fatigue crack initiates from a sharp crack. In the

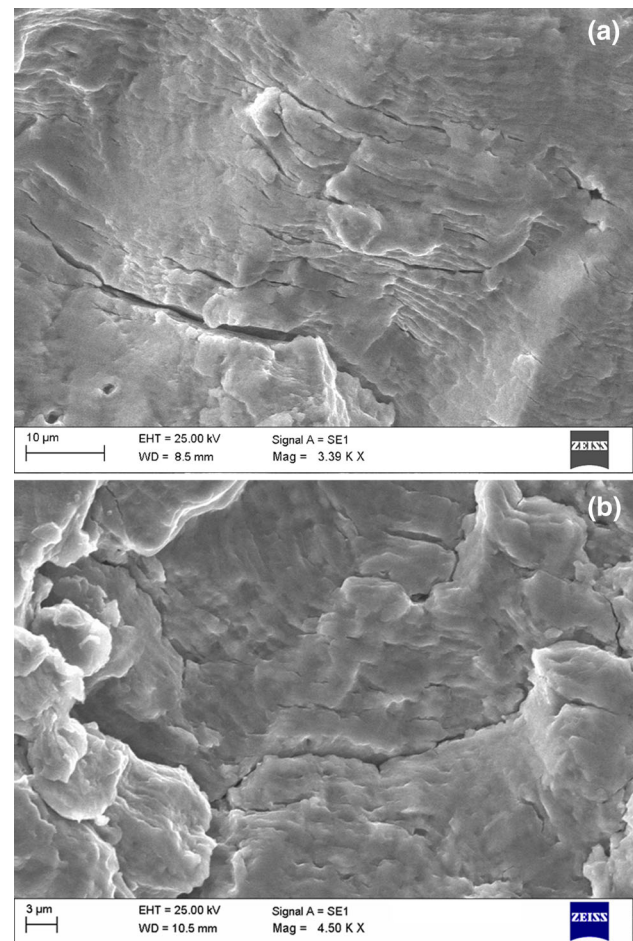
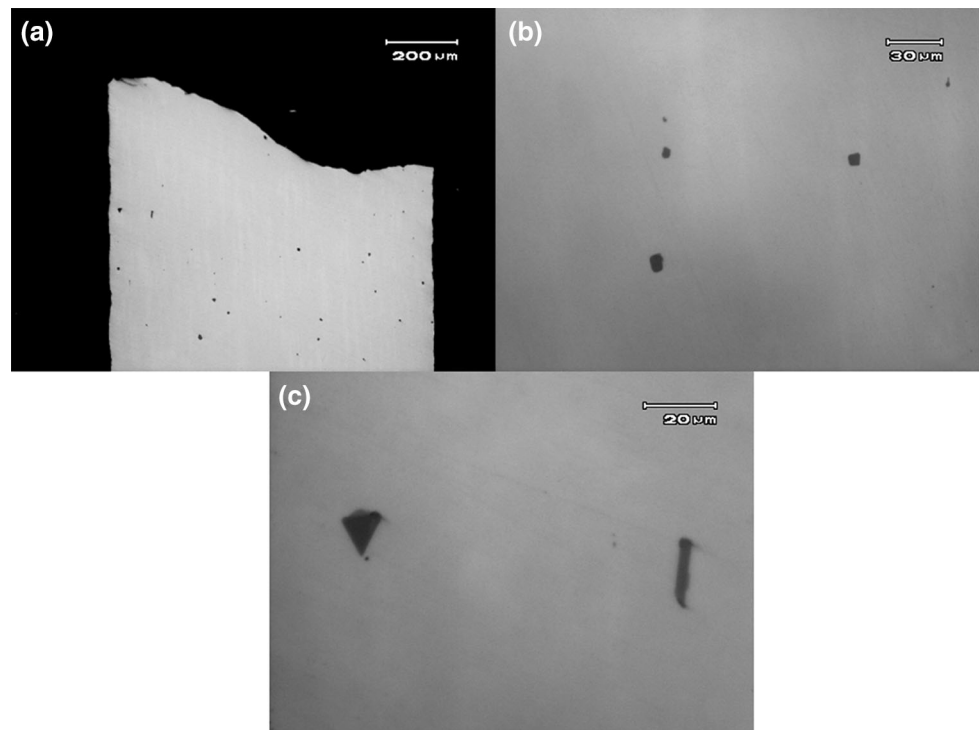


Fig. 14 SEM photograph showing the microcracks at the fatigue striations on fracture surface of Ø4 nipple

present case, the sharp-cornered inclusions were present in the material, which can easily initiate the crack or deviate the crack path as in case of Ø6 mm plumbing. The crack path deviation could be related to the presence of sharp inclusions at the path of primary crack.

The presence of micro crack in Ø6 mm tube joint near to the primary fracture surface at weld–parent interface could be due to the additional region of stress concentration. In Ø6 mm plumbing the weld bead thickness was about 3 times the parent tube wall thickness and it leads to the lower angle (105°) between weld bead and parent. This also resulted in less radius of curvature (66 µm) at weld–parent interface. In case Ø4 mm plumbing where the weld bead thickness was 1.5 times the parent tube wall thickness resulted in higher angle (150°) between weld bead and parent and higher radius of curvature (455 µm). In butt

Fig. 15 Optical photomicrographs showing the large nos. sharp-cornered inclusions present in the material $\text{\O}6$ nipple



welded joints, the angle at weld–parent interface is a measure of stress concentration at the interface and higher stress concentration reduces the fatigue strength [10]. The lower angle and less radius of curvature at the weld–parent interface increases the fatigue stress concentration factor [11, 12].

Cerit et al. [11] reported that for 120° angle and 0.5 mm radius at weld–parent interface, the stress concentration factor exceeds 3.3. Nascimento et al. [12] reported that for 127° angle and 0.42 mm radius, the stress concentration factor was higher than 3.4. Similar observations were made by Pardal et al. [13] in the failure of duplex stainless steel high pressure oil tube. In the present case, in $\text{\O}6$ mm plumbing joint, the angle (105°) and radius ($66 \mu\text{m}$) was much lower than the above reported literature and have increased the stress concentration factor significantly at weld–parent interface. This resulted in secondary fatigue crack initiation at weld–parent interface in addition to the primary fatigue crack at cross-section change area. The fractographic observations under SEM revealed that the fracture surface was predominantly covered with fatigue striations, indicative of fatigue failure. Some of the striated regions also indicated that secondary cracks were formed at the sharp-cornered inclusions. Slip bands observed at the fracture edge indicate the localised strain at fracture edge

due to fatigue. The plumbing tubes have already undergone resonance survey, sinusoidal vibration, and random vibration along two different axes before failure and failure occurred during third-axis random vibration test. It confirms that the tubes have experienced large cycles of fluctuating loads resulted in fatigue failure.

Conclusion and Recommendation

The plumbing tubes had experienced different types of fluctuating vibration loads and failed due to fatigue. The stress concentration arising out of cross-section change areas in the nipple region of the tubes was mainly responsible for early initiation of fatigue cracks in both the tubes. Sharp-cornered inclusions present in the steel could also have contributed for the crack initiation and crack path deviation in $\text{\O}6$ mm tube. The additional crack in the $\text{\O}6$ mm tube joint was due to the additional site of stress concentration at weld–parent interface because of lower angle and radius of curvature at weld–parent interface.

In order to avoid recurrence of such failures, it is recommended to maximize the radius at the cross-section change area to reduce the stress concentration. A good

Fig. 16 EDS spectrum showing the chemical composition of the inclusion on the fracture surface (a) and polished surface (b) of Ø6 nipple

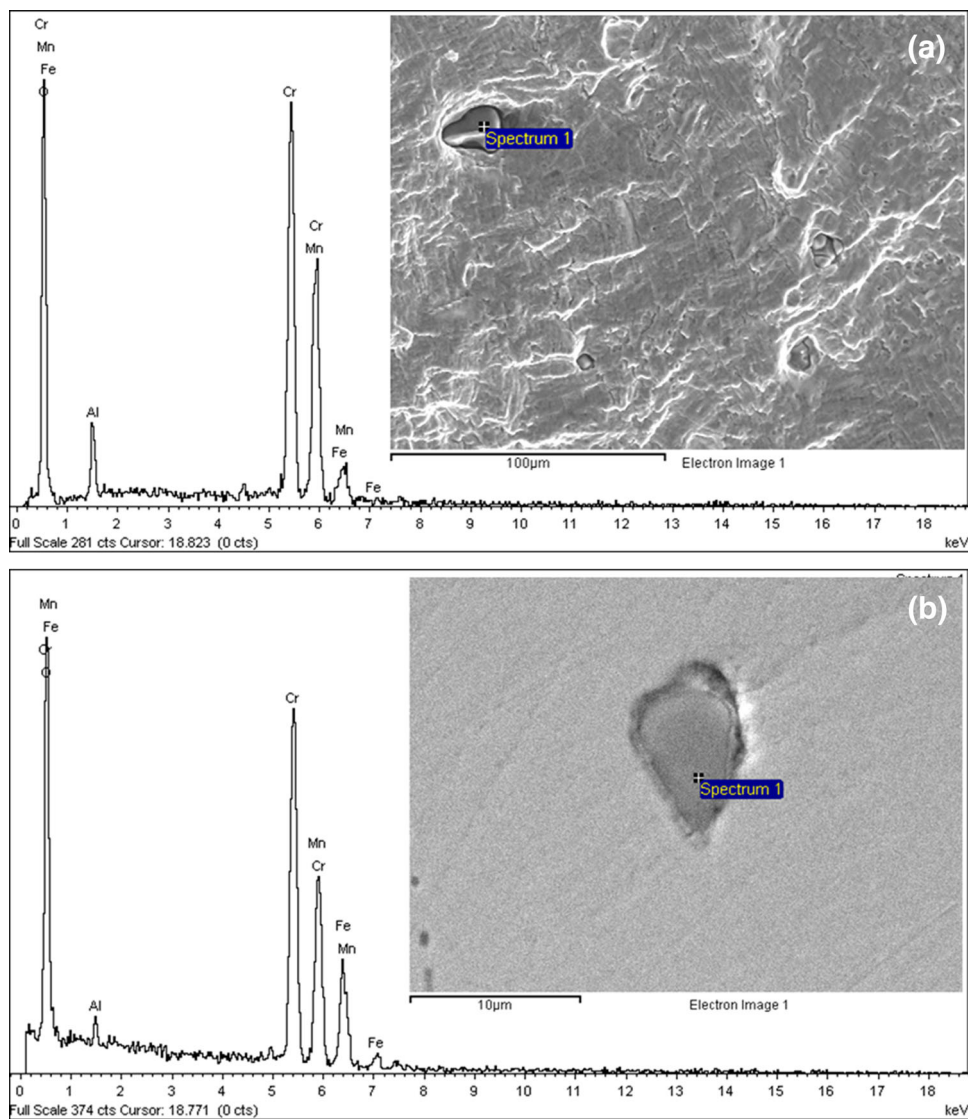


Fig. 17 Optical photomicrographs showing large variation in weld bead thickness between Ø6 mm (a) and Ø4 mm (b) tube joint

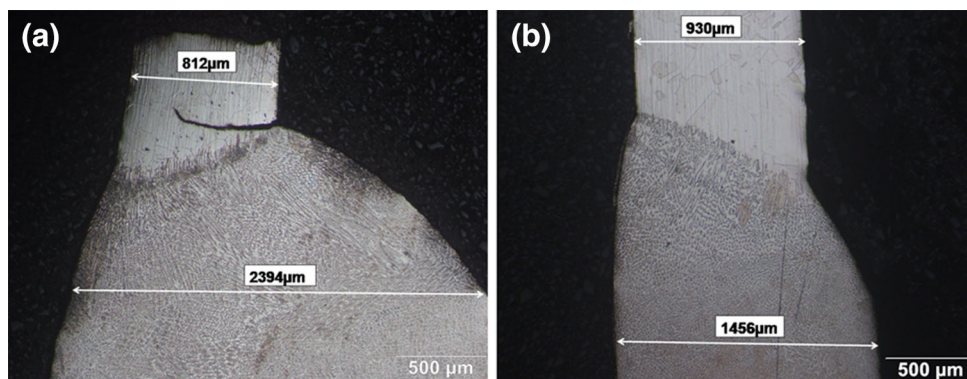


Fig. 18 Optical photomicrographs showing angle between weld bead and parent in Ø6 mm (a) and Ø4 mm (b) tube joint

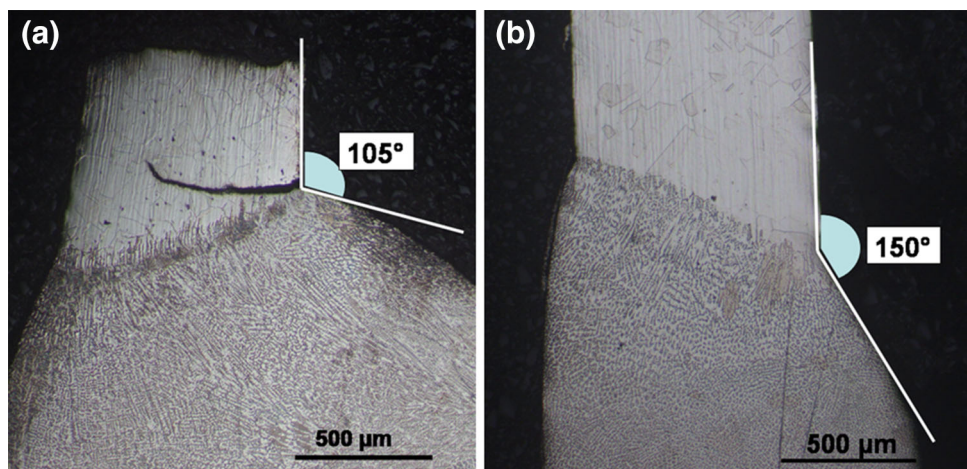


Fig. 19 Optical photomicrographs showing the radius at weld–parent interface in Ø6 mm (a) and Ø4 mm (b) tube joint

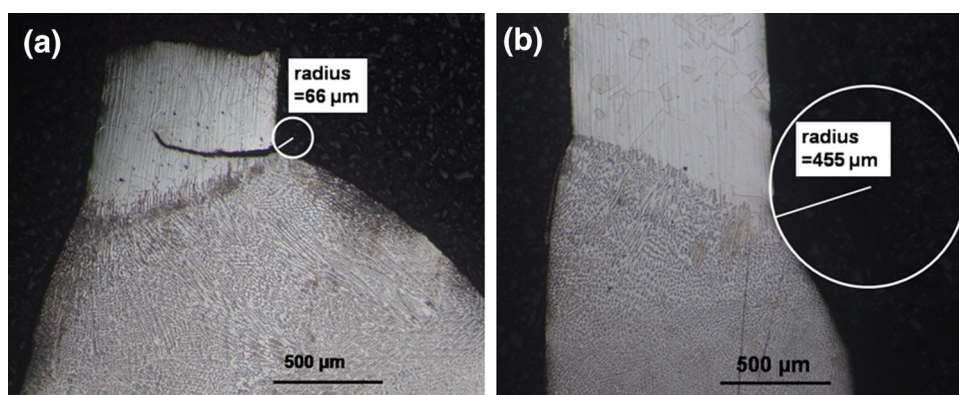
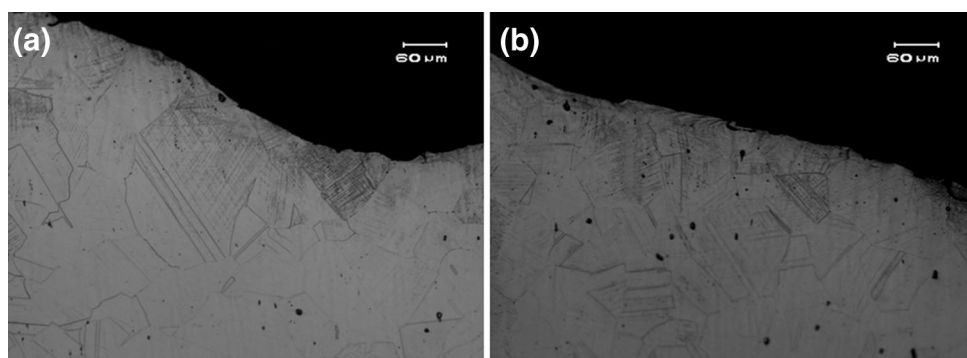


Fig. 20 Optical photomicrographs showing the presence of slip bands near to the fracture edge of Ø6 nipple



surface finish at the cross-section change area should be ensured and should be free of tooling marks. Alternatively, the design of the tube joint can be modified to remove the cross-section change. A sufficiently large radius and angle should be ensured at weld–parent interface to reduce the stress concentration at weld joint. The raw material used for fabricating tubes should be microstructurally cleaner with respect to the sharp-cornered inclusions as they contribute to easy crack initiation are more detrimental to the fatigue loading conditions.

Acknowledgments Authors wish to thank Director, VSSC for his kind permission to publish this work. They further wish to thank ESCD, LPSC Valiamala for referring the analysis and for supplying the specimens.

References

1. W.F. Smith, *Structure and Properties of Engineering Alloys*, 2nd edn. (McGraw Hill Inc., New York, 1993), pp. 312–322
2. M. Kutz, *Handbook of Materials Selection* (Wiley, New York, 2002), p. 59

3. J.A. Brooks, Selection of wrought austenitic stainless steel, in *ASM Handbook Volume 6: Welding, Brazing and Soldering* (ASM International, Materials Park, 1993)
4. R. Kiessling, *Non-metallic Inclusions in Steel* (The Metals Society, London, 1978). ISBN 0-904357-18-X
5. J. Cheng, R. Eriksson, P. Jönsson, Determination of macroinclusions during clean steel production. *Ironmak. Steelmak.* **30**(1), 66–72 (2003)
6. W.E. Duckworth, E. Ineson, The effects of externally introduced alumina particles on the fatigue life of En24 steel. *Clean Steel Iron Steel Inst. Spec. Rep.* **77**, 87–103 (1963)
7. S. Nishijima, K. Tanaka, H. Sumiyoshi, The defect size determining the fatigue limits of steels, in *Advances in Fracture Research (Fracture 84)*, vol. 3, New Delhi, India, 4–10 Dec. 1984 (Pergamon Press Ltd., Oxford), pp. 1719–1726
8. A. Melander, P. Ölund, Detrimental effect of nitride and aluminium oxide inclusions on fatigue life in rotating bending of bearing steels. *Mater. Sci. Technol.* **15**(5), 555–562 (1999)
9. J. Schijve, The practical and theoretical significance of small cracks. An evaluation, in *Fatigue'84, Proceedings of the 2nd International Conference on Fatigue, Birmingham, 3–7 Sept. 1984*, vol. 2 (EMAS, Warley, 1984), pp. 751–771
10. J.F. Lancaster, *Metallurgy of Welding*, 6th edn. (Abington Publishing, Abington, 1999), p. 240
11. M. Cerit, O. Kokumer, K. Genel, Stress concentration effects of undercut defect and reinforcement metal in butt welded joint. *Eng. Fail. Anal.* **17**(2010), 571–578 (2010)
12. M.P. Nascimento, H.J.C. Voorwald, J.D.C. Payao Filho, Fatigue strength of tungsten inert gas-repaired weld joints in airplane critical structures. *J. Mater. Process. Technol.* **211**(2011), 1126–1135 (2011)
13. J.M. Pardal, G.C. de Souza, E.C. Leao, M.R. da Silva, S.S.M. Tavares, Fatigue cracking of high pressure oil tube. *Case Stud. Eng. Fail. Anal.* **1**(2013), 171–178 (2013)